Influence of the machining cooling strategies on the dental tribocorrosion behaviour of wrought and additive manufactured Ti6Al4V

Biotribology 11 (2017) 60–68

Contents lists available at ScienceDirect

Biotribology

journal homepage: www.elsevier.com/locate/biotri

Influence of the machining cooling strategies on the dental tribocorrosion behaviour of wrought and additive manufactured Ti6Al4V

R. Bertolini[a,*], S. Bruschi[a], A. Ghiotti[a], L. Pezzato[b], M. Dabalà[b]

[a] University of Padova, Department of Industrial Engineering, Via Venezia 1, 35131 Padova, Italy
[b] University of Padova, Department of Industrial Engineering, Via Marzolo 9, 35131 Padova, Italy

1. Introduction

Titanium and its alloys are the most widely used implant materials due to their high corrosion resistance in biological environments, good strength-to-weight ratio, and excellent biocompatibility [1,2]. They are characterized by a protective passive film that is responsible for their chemical stability, corrosion resistance and fast repassivation in a wide range of environments. However, despite their attractive corrosion properties, they generally exhibit poor wear resistance [3]. In fact, when used as implants, cyclic micro-movements at the implant/bone interface or implant/abutment interface may occur, inducing significant wear [4,5], which, together with the chemical interactions with the environment, can lead to the destruction of the repassivation protective layer causing a progressive material loss and release of harmful metal debris inside the human body, forcing to a premature replacement of the implant [6–8].

Tribocorrosion can be defined as the degradation of a tribological contact resulting from the combined effect of the metal removal by mechanical wear and by electrochemical oxidation. To this regard, each chewing process can be regarded as a tribocorrosion cycle since sliding occurs between the tooth and the food particles in presence of corrosive saliva [9]. The repeated removal of the oxide films induced by the chewing cycles produces wear at the implant/abutment interface leading to adverse biological reactions and, possibly, to the mechanical failure of the device.

Several recent literature studies have focused on the tribocorrosion behaviour of titanium alloys. Licausi [10] et al. studied the influence of different PHs on the tribocorrosion behaviour of the Ti6Al4V titanium alloy obtained by two different fabrication processes, namely casting and powder metallurgy. They carried out ball-on-flat disc reciprocating sliding wear tests in solution with different pHs, proving that the cast and sintered Ti6Al4V exhibited the same tribocorrosion behaviour. Souza et al. [11] studied the effect of applying a bio-absorbable polymer coating on the Ti6Al4V surface to improve the tribocorrosion behaviour: the obtained results showed a lower Coefficient Of Friction (COF) on the coated Ti6Al4V compared to the uncoated one and also a decrease in the wear rate. Hacisalihoglu et al. [12] investigated the tribocorrosion behaviour of α and α-β titanium alloys in Simulated Body Fluids (SBF), finding that the latter alloys had a superior behaviour in terms of lower COF and volume loss compared to the α alloys.

Alternative processing routes are being widely studied for manufacturing biomedical implants. To this regard, recent studies have dealt with the investigation of innovative manufacturing techniques, such as powder metallurgy and Additive Manufacturing (AM), in order to improve the material biomedical performances. As example, Doni et al. [13] compared the cast CoCrMo with the same alloy obtained through a powder metallurgy method: they tested both the materials in a saline environment at room and body temperature in a reciprocating sliding wear regime, finding that, although both the CoCrMo alloys presented similar behaviour in term of COF and Open Circuit Potential (OCP), the wear rate of the hot pressed material was three times lower than the one of the cast alloy.

At the same time, other different processing techniques are being investigated to increase the wear resistance of the titanium alloys. The use of cryogenic cooling during machining has been demonstrated to be an effective mean to enhance the surface properties of implant devices. The relevance of the cooling strategy in machining Ti6Al4V produced by AM was recently pointed out in [14], where it was proved that the application of liquid nitrogen led to an improvement of the machined surface integrity by reducing the microstructural alterations. Rotella et al. [15] demonstrated the capability of cryogenic cooling to improve the product surface integrity in machining Ti6Al4V: they found that the cryogenically machined samples showed a superior surface finishing leading to an increase in the micro-hardness at a surface and subsurface level and to the grain size decrease. Umbrello et al. [16] studied the effect of using liquid nitrogen as coolant in comparison to dry conditions when machining an hardened AISI 52100 steel focusing on the surface integrity: they found that the use of cryogenic cooling limited the formation of the white layer and generated a better surface roughness leading to an enhancement of the product service life.

Bruschi et al. [17] studied the influence of machining parameters and cooling strategies on the reciprocating sliding wear behaviour of the Ti6Al4V alloy delivered in two conditions, namely wrought and AM

* Corresponding author.
E-mail address: rachele.bertolini@dii.unipd.it (R. Bertolini).

http://dx.doi.org/10.1016/j.biotri.2017.03.002
Received 30 October 2016; Received in revised form 6 March 2017; Accepted 16 March 2017
Available online 11 May 2017

by Electron Beam Melting (EBM). They found that cryogenic machining was an efficient method to reduce friction and to assure the occurrence of a higher degree of adhesive wear, proving, therefore, an improvement of in-vitro implant performances.

Bertolini et al. [18] investigated the effect of the cutting parameters and cooling strategies on the fretting corrosion behaviour of the EBM Ti6Al4V alloy, replicating the same conditions of the taper interfaces of a modular hip junction. They stated that cryogenic machining was the most effective cutting strategy that could enhance the mechanical, chemical, and tribological behaviour of the machined surfaces.

On the basis of the literature review and with the aim of improving the tribocorrosion behaviour of the Ti6Al4V used in dental applications, in this research study different cooling strategies were applied in machining wrought and AM Ti6Al4V samples and their influence on the alloys tribocorrosion behaviour was investigated and critically assessed.

2. Experimental

2.1. Materials

The wrought Ti6Al4V samples were machined into cylinders from a commercially available annealed bar of 30 mm diameter and 200 mm of height.

The AM Ti6Al4V samples were machined into cylinders from a cylindrical billet produced by Electron Beam Melting (EBM) using an ARCAM™ Q10 machine. Each billet was manufactured with the symmetry axis parallel to the growing direction, with a diameter of 30 mm and a height of 180 mm.

Both the wrought and EBM Ti6Al4V machined cylinders had a diameter of 20 (± 0.02) mm and a length of 5 (± 0.02) mm.

The Ti6Al4V cylinders were made to slide against zirconia plates in order to recreate an actual biotribological pair. The zirconia ZrO_2 was chosen as counterpart material because it is commonly used for the fabrication of dental implant abutments [19].

The mechanical properties of the materials used in this study are given in Table 1.

2.2. Machining tests

The machining tests were conducted on a Mori Seiki™ CNC lathe equipped with a special designed line assembled to fulfil the cryogenic cooling. The cryogenic fluid used in the tests was Liquid Nitrogen (LN_2), supplied to the cutting zone from a high pressure storage dewar through a vacuum insulated pipe; the supplying pressure was set to 15 bars.

As can be seen in Fig. 1, two cylindrical copper nozzles with an internal diameter of 0.9 mm were used to direct the LN2 simultaneously towards the tools flank and rake faces to improve its cooling capacity [20]. The nozzles were positioned approximately 4 mm from the tip of the insert, and the directions of LN_2 was set equal to 45° with the respect to the tip of the cutting tool. This configuration was optimized in order to have the reduction of temperatures of the entire cutting zone, both of the workpiece and cutting tool. For the latter, a reduction in adhesive wear due to the intense cooling capacity of the liquid nitrogen and limitation in abrasive wear of both the cutting edge and flank face were achieved in the case of cryogenic cooling. Further details on the cryogenic cooling apparatus and its effect on machinability can be found in [14].

Table 1
Ti6Al4V and ZrO_2 mechanical characteristics in the as-delivered state.

Ti6Al4V				
As-delivered state	E [GPa]	Y [MPa]	UTS [MPa]	HRC
Wrought	118	790	872	33
EBM	120	950	1020	31

ZrO_2		
Material	E [GPa]	K_{IC} [MPa/m$^{0.5}$]
Zirconia ZrO_2	210	10

The adopted cutting tool was a semi-finishing coated tungsten carbide insert CNMG1-20404SM-GC1105 (substrate composition: 93% WC and 7%Co) with a radius of 0.4 mm, mounted on a PCLNR/L tool holder with an approach angle of 75°, both supplied by Sandvik Coromant™. The cutting tool consisted of a fine grain WC substrate, giving good heat and plastic deformation resistance; while the coating consisted of a TiAlN layer deposed by PVD, allowing good toughness, uniform flank wear, and overall high machining performances. The resultant rake and clearance angles were equal to 7° and 0°, respectively. Both the insert grade and micro geometry were chosen on the basis of the tool manufacturer's advices for machining titanium alloys. In order to avoid the influence of the tool wear on the surface topography of the machined cylinders, a fresh cutting edge was adopted for each test. The values of the cutting speed (Vc) and feed rate (f) adopted for the tests, namely 80 m/min, and 0.1 mm/rev, respectively, were chosen on the basis of previous studies [18]. The depth of cut (d) was maintained constant and equal to 0.25 mm in order to achieve a semi-finishing cutting condition.

The machining tests were performed with three different cooling conditions, namely, dry, wet and cryogenic. While dry and wet machining are established methods, the cryogenic one may represent an innovative efficient solution for machining biomedical components thanks to the advantages it offers. In fact, this cooling strategy allows the reduction of the cutting temperature by supplying LN_2 directly on the cutting zone, permitting the adoption of more severe cutting parameters. Moreover, LN_2 gasifiers during machining, leaving the workpiece clean and dry, hence reducing the cleaning steps to which biomedical surgical implants are subjected when adopting standard emulsion cooling [14].

The experimental plan for the machining tests is reported in Table 2.

2.3. Surface characterization after machining

After the machining tests, the surface roughness of the Ti6Al4V samples was evaluated using a Sensofar Plu Neox™ surface profiler with a resolution of less than 20 nm on the optical *Z*-axis. Two roughness parameters were evaluated, namely the average roughness, Ra, and the mean roughness depth, Rz. Both the Ra and Rz measurements were evaluated along the perpendicular direction with the respect to the turning feed marks. Each reported value is the average result of six different measurements.

The zirconia plates were ground to obtain an initial surface roughness equal to 0.02 ± 0.09 μm.

Vickers micro-hardness measurements were performed using a Leitz Durimet™ micro-hardness tester with a load of 50 g (± 0.5) gr and a dwell time of 15 s; these parameters were chosen according to literature [21]. Five values were recorded for each machined cylinder and then the average value calculated. With the aim of studying the machining effect, the measurements were carried out at a distance of 30 μm from the machined surface.

The residual stresses on the cylindrical machined surfaces were measured by means of the X-Ray Diffraction (XRD) technique using the sin2ψ method. The XRD analysis was carried out on an Enixè™ TNX diffractometer, using CuKα radiation at 85 μA and employing 9 tilt angles (ψ). The residual stresses along the axial and circumferential directions with respect to the cylinder axis were measured on the machined surface (depth = 0 μm).

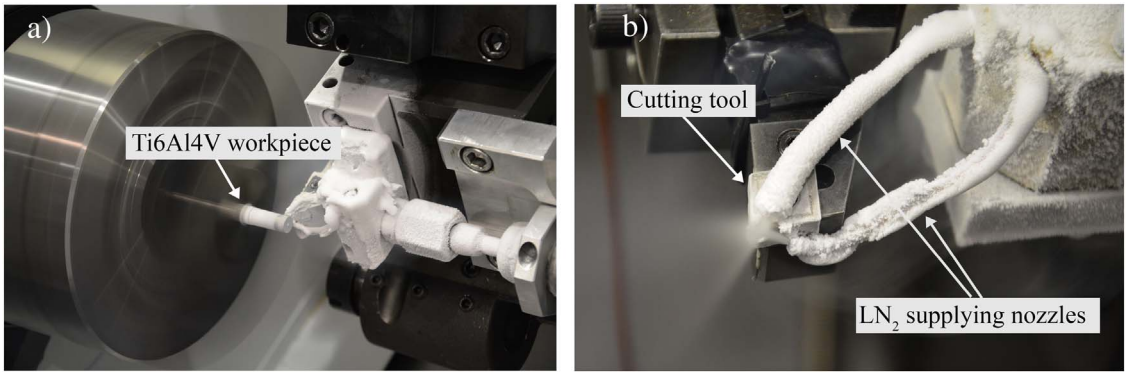

Fig. 1. a) Experimental set-up for the cryogenic turning of the Ti6Al4V samples; b) magnified photo of the liquid nitrogen delivery apparatus.

Table 2
Experimental plan for the machining tests.

Ti6Al4V as-delivered state	Cutting condition
Wrought	Dry
EBM	Dry
Wrought	Wet
EBM	Wet
Wrought	Cryogenic
EBM	Cryogenic

2.4. Corrosion tests

The electrochemical behaviour was studied using a standard three electrodes cell, where the Ti6Al4V machined samples were the working electrode, a saturated Calomel electrode (SCE) the reference electrode, and a platinum electrode the counter electrode. The Amel™ 2549 potentiostat was used for the electrochemical tests. The Ti6Al4V samples were first immersed in the electrolyte for 60 min under OCP for stabilising the potential. Then, the potentiodynamic polarization curves were obtained applying a potential from − 0.8 V to 1.7 V at a scan rate of 0.5 mVs^{-1}. The potentiodynamic polarization curves were obtained through testing in artificial saliva, whose composition was 0.4 g NaCl, 0.4 g KCl, 0.6 g $CaCl_2$, 0.58 g Na_2HPO_4*$12H_2O$, 1 g urea, distilled water at 1 L, at body temperature (37 ± 1 °C), in order to reproduce the human mouth conditions. The corrosion potential (Ecorr) and the corrosion current density (Icorr) were determined from the polarization measurements using the Tafel extrapolation method, according to the ASTM G5-14 standard. The potentiodynamic polarization curves were repeated twice in order to assure the results reproducibility.

2.5. Biotribological tests

Reciprocating sliding corrosion experiments were carried out coupling an electrochemical cell (Fig. 2a) to the Rtech™ Instruments tribometer equipped with an integrated optical profiler. The employed contact configuration consisted in a Ti6Al4V cylinder, mounted on a non-conductive holder, sliding against a ZrO_2 flat-plate. The cylinder-on-flat configuration, shown n Fig. 2b), was selected as it was the most suitable to investigate the behaviour of cylindrical shapes obtained by turning. The schematic representation of the overall experimental set-up is reported in Fig. 2c).

The contact interface was immersed in artificial saliva constantly maintained at a temperature of 37 ± 2 °C. A thermometer, immersed in the water basin, was used to have a feedback of the temperature in the solution. The experiments were performed at a frequency of 1 Hz and lasted 3600 s. A normal force of 45 N was applied, which resulted in an initial contact pressure of 220 MPa on the basis of the results of a previous literature work [22]. A stroke of 1 mm was imposed. In order

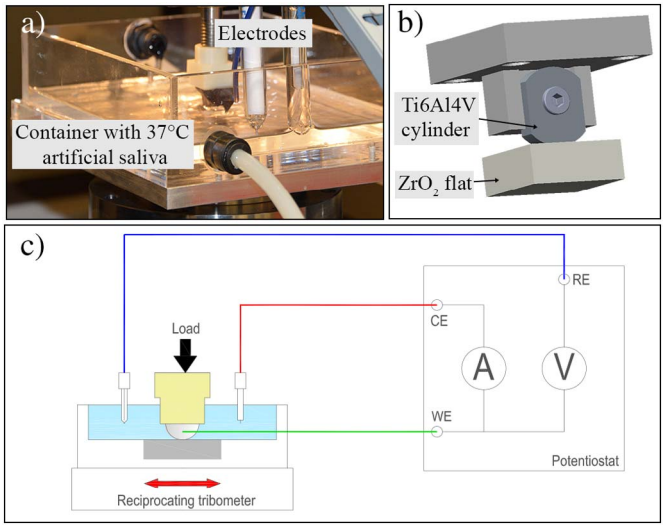

Fig. 2. a) Tribometer equipped with an electrochemical cell placed on the container of heated artificial saliva; b) scheme of the cylinder-on-flat configuration; c) scheme of the overall tribocorrosion apparatus.

to assure the full contact of the entire cylinder length, a profiler scan was performed before starting the tests.

The sliding tests were carried out both at OCP and at an applied passive potential of 0.2 V.

The experimental sequence adopted for the biotribological tests was the following:

- Either system stabilisation at OCP for 5 min or application of the selected potential.
- Sliding for 60 min while continuous measurement of either the OCP or the current.
- Removal of the load while keeping constantly measured the OCP for 5 min or constantly applied the established potential.

For each condition, tests were repeated three times in order to assure the results repeatability.

2.6. Wear characterization

After the biotribological tests, the volumetric wear was evaluated using the Sensofar Plu Neox™ profiler. Three different profiles of the wear track were measured in the area characterized by the maximum pressure, which is located at the middle of the reciprocating sliding path at a distance of ± 1 mm from the centre. The average cross section worn area was then multiplied by the wear track length in order to assess the wear volume.

A Quanta™ FEI Scanning Electron Microscopy (SEM) equipped with

Table 3
Surface characteristics of the wrought and EBM Ti6Al4V cylinders after semi-finishing turning.

Ti6Al4V as-delivered state	Cutting condition	Ra [μm]	Rz [μm]	$HV_{0.05}$	σa [1]	$σt^2$
Wrought	Dry	0.365 ± 0.005	2.044 ± 0.11	364 ± 6	− 50	− 208
EBM	Dry	0.354 ± 0.009	1.931 ± 0.18	370 ± 4	− 28	− 205
Wrought	Wet	0.358 ± 0.008	1.934 ± 0.07	371 ± 5	− 55	− 150
EBM	Wet	0.351 ± 0.009	2.212 ± 0.22	380 ± 3	− 71	− 160
Wrought	Cryogenic	0.341 ± 0.035	1.693 ± 0.27	391 ± 8	− 67	− 108
EBM	Cryogenic	0.326 ± 0.019	1.76 ± 0.11	400 ± 5	− 87	− 148

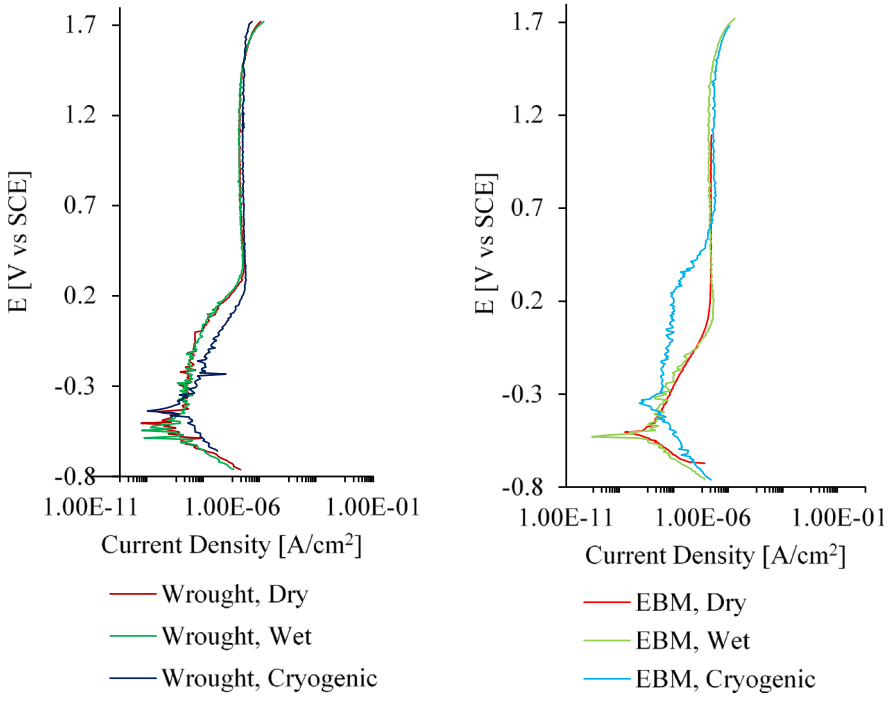

Fig. 3. Potentiodynamic polarization curves in artificial saliva at 37 °C: (a) wrought Ti6Al4V, and (b) EBM Ti6Al4V.

the Everhart-Thornley Detector (ETD) and Backscattered Electron (BSED) detectors was used to analyse the worn cylinder surfaces.

3. Results

3.1. Surface characterization after machining

The results of the surface integrity characterization for the EBM and wrought Ti6Al4V cylinders are presented in Table 3.

σa [1] = residual stress along the axial direction, $σt^2$ = residual stress along the tangential direction.

As expected, the material as-delivered conditions have a slight influence on the surface roughness. On the contrary, the cooling strategy has an important effect, considerably affecting the surface finish. The use of LN_2 as coolant leads to smoother surfaces, dry machining to rougher surfaces whereas the wet condition sets in the middle. The same trend can be found in the work of Dhananchezian et al. [23] where the influence of the cooling conditions on the surface integrity of the wrought Ti6Al4V was studied: they attributed the surface roughness reduction to the decreased cutting temperature that led to less adhesion forces between the newly generated workpiece and the tool surface resulting in lower tool wear.

On the contrary, the roughest surface was obtained with dry cutting as a consequence of the high temperature reached on the workpiece and the high friction at the workpiece-tool interface [24].

In general, the use of different cooling strategies causes a variation of the micro-hardness regardless of the Ti6Al4Vas-delivered conditions, with values higher for the EBM Ti6Al4V compared to the wrought one. The highest hardness was recorded in all the cryogenic machined samples, with an increase up to 8% compared to the dry condition. The wet machined samples performed better than the dry machined ones, but had a lower hardness compared to the cryogenic machined samples. The use of the cutting fluid reduced indeed the temperature, although the cooling effect was not comparable with that assured by the use of the LN_2.

The measurements of the residual stresses pointed out that the use of the cryogenic cooling induced higher compressive residual stresses at the surface along the axial direction, while, on the contrary, dry machining generated higher compressive residual stresses along the tangential direction. Again, the wet condition sets in the middle. Outeiro et al. [25] studied the influence of cryogenic machining on the surface and subsurface residual stresses distribution finding that this cooling strategy could induce a slightly deeper compressive residual stress profile when compared to dry cutting especially near the surface where the material was more significantly affected by the heating generated during machining. Pusavec et al. [26] studied the surface integrity of the Inconel 718 as function of the cooling conditions, namely dry, minimum quantity lubrication and cryogenic cooling. They found that in case of cryogenic cooling not only the stresses beneath the surface decreased up to 60%, but also the affected zone was thicker.

Therefore, it can be concluded that cryogenic machining can lead to a substantial improvement in the surface finish parameters leading to a harder, smoother and more compressed surface.

Table 4
Corrosion potentials and corrosion current densities recorded in artificial saliva at 37 °C.

Ti6Al4V as-delivered state	Cutting condition	I_{CORR} [mA/cm^2]	E_{CORR} [V]
Wrought	Dry	8E − 08	− 0.5
EBM	Dry	3E − 08	− 0.55
Wrought	Wet	9E − 08	− 0.5
EBM	Wet	3E − 08	− 0.5
Wrought	Cryogenic	2E − 08	− 0.4
EBM	Cryogenic	1E − 08	− 0.35

3.2. Corrosion curves

The potentiodynamic polarization curves obtained in artificial saliva at 37 °C are reported in Fig. 3. Table 4 shows the electrochemical parameters extracted from the potentiodynamic curves of the wrought and EBM Ti6Al4V as function of the different cooling conditions.

By comparing the polarization curves, it can be noted that, regardless of the Ti6Al4V as-delivered conditions, all the cryogenic machined samples presented curves that were shifted towards higher potentials, with an ennoblement of about 0.2 V in case of the EBM Ti6Al4V, and an ennoblement of about 0.1 V for the wrought Ti6Al4V. The corrosion potential is a thermodynamic characteristic related to the material tendency of being corroded and is a measure of the nobility of the sample [27]: the cryogenic machined samples characterized by higher E_{corr} were less likely attacked by the corrosion environment than the dry machined samples characterized by lower E_{corr}.

Considering instead the EBM alloy, a much more significant decrease in the corrosion current density, and so an increase in the corrosion resistance, can be observed.

In terms of corrosion current density, there was a slight decrease for the cryogenic machined samples compared to the dry and wet ones in case of the wrought alloy. As claimed in the G102-89 standard [28], the I_{corr} is linked through a directly proportional relationship to the corrosion rate; this means that an increase in I_{corr} corresponds to an increase in the mass lost by the Ti6Al4V implant during its service-life in the human body.

This indicates that the corrosion properties are strongly influenced by the cooling conditions, proving that cryogenic machining can be an efficient method for enhancing the material corrosion properties. In addition the material as-delivered state significantly influences the corrosion resistance: in fact, the EBM alloy is characterized by improved corrosion properties than the wrought one, thus being for the EBM alloy the cooling effect more significant. A nobler potential together with lower corrosion current density implies that the material is characterized by a better corrosion behaviour, which is a highly demanded characteristic in the case of aggressive environment like the human mouth. Thus can be ascribed to the obtained surface conditions, and, in particular, to the high compressive stress state recorded along the axial direction on the surface of the cryogenic machined samples. The strong correlation between the compressive residual stresses and the improved corrosion performances can be found in different literature works. Takakuwa et al. [29] studied the effect of the residual stresses generated by different surface finishes on the corrosion behaviour of the austenitic stainless steel 316L finding a strong correlation between the two factors. In particular, they found a rapid decrease up to 70% in the current density at increasing the compressive residual stresses. They ascribed this enhanced behaviour to the formation and retention of a passive film that required lower current density when a compressive stress was introduced in the material. These results are confirmed by the studies carried out by Y. Wang [30] who reported that the surface integrity had a significant effect on the corrosion resistance of an aluminium alloy, finding a decrease in corrosion pits when a compressive residual stress state was induced in the material.

Therefore, it can be concluded that cryogenic cooling can be used as a strategy to strengthen the Ti6Al4V corrosion resistance in human mouth corrosive media.

3.3. Biotribological results

The evolution of the OCP with time of the titanium alloys was monitored before, during and after the sliding tests. The obtained results are reported in Fig. 4.

Before the beginning of the sliding, the measured OCP indicates the presence of a passive film on the alloy surface in contact with the saliva solution. An anodic shift was observed suggesting a thickening of the passive layer. An abrupt decrease of the potential was observed after the starting of the test, indicating a depassivation of the surface induced by the scratching of the passive film caused by sliding and, therefore, indicative of the exposure of fresh active titanium to the environment. The OCP reached a minimum value immediately after the beginning of the test and then it tended to increase towards less active values as a consequence of the equilibrium reached between the mechanical depassivation and the electrochemical repassivation. The small oscillations of the OCP during sliding are indicative of this phenomenon of scratching and subsequent reformation of the passive layer. At the end of the sliding, the OCP recovered towards more positive values indicating the reformation of the passive layer on the material. The values of the average potential recorded during the reciprocating sliding tests are reported in Table 5.

The average potential values that characterized the wrought

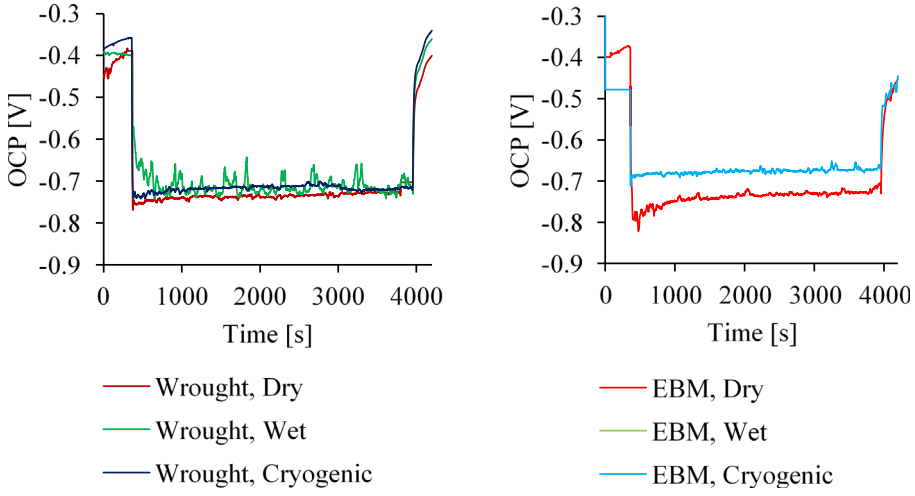

Fig. 4. OCP evolution with time during the biotribological tests in artificial saliva at 37 °C: a) wrought Ti6Al4V, and b) EBM Ti6Al4V.

Table 5
Potential (E_{AVG}) and corrosion current ($I_{sliding}$) recorded during the biotribological tests.

Ti6Al4V as-delivered state	Cutting condition	E_{AVG} (mV)	$I_{sliding}$ (μA)
Wrought	Dry	− 71 ± 9	107 ± 26
EBM	Dry	− 73 ± 5	135 ± 24
Wrought	Wet	− 69 ± 5	122 ± 24
EBM	Wet	− 72 ± 2	107 ± 24
Wrought	Cryogenic	− 69 ± 9	105 ± 26
EBM	Cryogenic	− 67 ± 5	75.1 ± 80

Ti6Al4V were slightly higher than those of the EBM alloy. This outcome seems to be in disagreement with the results of the surface characterization after machining; however, similar evidences are present in literature, like the work by Licausi et al. [10] who studied the corrosion and tribocorrosion behaviour of the Ti6Al4V obtained by casting and powder metallurgy, and found that the cast alloy tribocorrosion curves set at higher potential values compared to the ones of the sintered alloy. They ascribed such behaviour to the presence of pores that increased the sintered alloy surface exposed to the test solution.

Concerning the different cooling conditions, the dry machined samples were characterized by the lowest potential values while the cryogenic machined curves were generally arranged to higher potential values. This means that, during naturally scratches of dental implant in oral mouth as tested in this study, the cryogenic machined samples are less prone to be corroded. Again, the samples machined using the cutting fluid had an intermediate behaviour between the dry and the cryogenic machined ones. The potential sensitivity to the cooling conditions is in agreement with the results of the machined surface characterization, proving that the higher the hardness and compressive residual stresses the more improved the corrosion resistance. To this regard, the EBM sample that was cryogenically machined showed the best performance in terms of corrosion resistance. Therefore, the OCP monitoring during the biotribological tests substantially confirmed the results recorded during the potentiodynamic polarization: the cryogenic machined samples had the best corrosions performances, even more evident in case of the EBM Ti6Al4V.

Fig. 5 shows the current density evolution with time when a constant potential of 0.2 V was applied during the biotribological tests. Before the sliding starting, the whole surface was passive and the anodic current was very low. When the sliding started, a sudden increase of the current occurred due to the mechanical removal of the oxide layer and the anodic dissolution of the surface active sites. At the end of the test, the current dropped since the mechanical removal effect was suppressed allowing the reformation of the oxide layer at the worn area. Table 5 summarizes the average values of the current density assumed by the samples during the biotribological tests carried out at an applied passive potential. The current passing during sliding was calculated by subtracting the value of the current measured before starting the test from the current measured during sliding. Again, the most influencing parameters were the cooling conditions, showing that the dry machined samples were characterized by the highest current density while the cryogenic machined ones were characterized by the lowest value. The considerations proposed for explaining the OPC test can be similarly applied in this case and this data confirm the previously reported ones.

According to Bazzoni et al. [31], in a tribocorrosion system several mechanisms simultaneously take place resulting in material volume loss: wear accelerated corrosion (leading to a volume loss referred to as V_{chem}) and mechanical removal of the particles (V_{mech}) in the wear track as well as corrosion (V_{corr}) outside the wear track. Therefore, the overall volume loss can be expressed according to Eq. (1):

$$V_{tot} = V_{mech} + V_{chem} + V_{corr}$$

Titanium alloys are prone to passivation and show very low passive dissolution rate; therefore, their volume loss caused by the corrosion outside the wear track can be neglected, and the overall material loss can be simplified as follows:

$$V_{tot} = V_{mech} + V_{chem}$$

The material removed by anodic oxidation in the wear track V_{chem} was calculated from the measured current values using the Faraday's law (3):

$$V_{chem} = \frac{I_{sliding} * t * M}{n * F * \rho}$$

where M is the atomic mass of the alloy (46.64), n the charge number for the oxidation reaction (assumed equal to 4), F the Faraday's constant (96,487 C/mol), ρ the density of the alloy (4.43 g/cm^3), and t the duration of the sliding equal to 3600 s.

The total wear volume was determined on the basis of the procedure described in Section 2.6. Fig. 6 A) shows the image of the worn surface of the wrought sample machined in dry condition acquired through the profiler, while Fig. 6 B) shows the matching graph of the wear scar in the area highlighted by the arrows. The obtained results are listed in Table 6, being the amount of V_{mech} the result of the difference between V_{tot} and V_{chem}.

In case of OPC just the total wear volume is reported, as the wear-

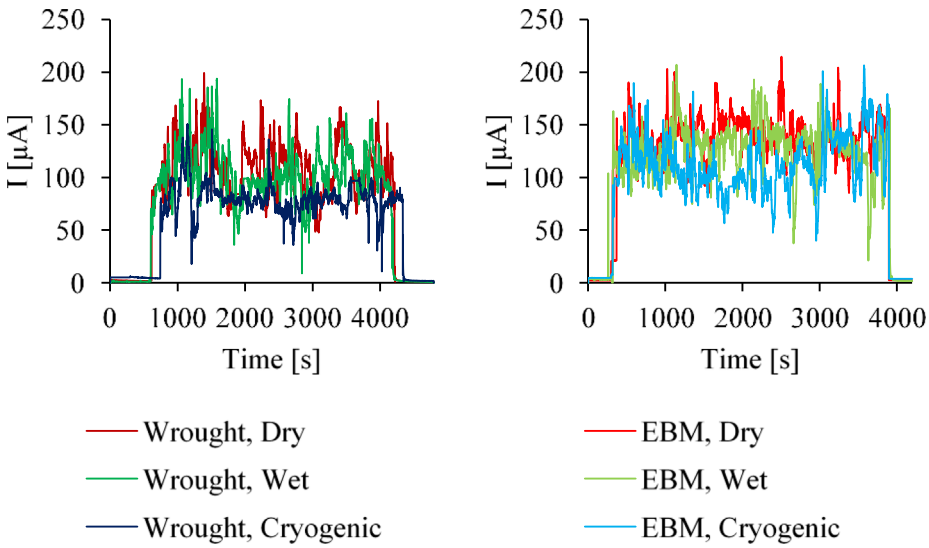

Fig. 5. Current evolution with time at an applied potential of 0.2 V in artificial saliva at 37 °C: a) wrought Ti6Al4V, and b) EBM Ti6Al4V.

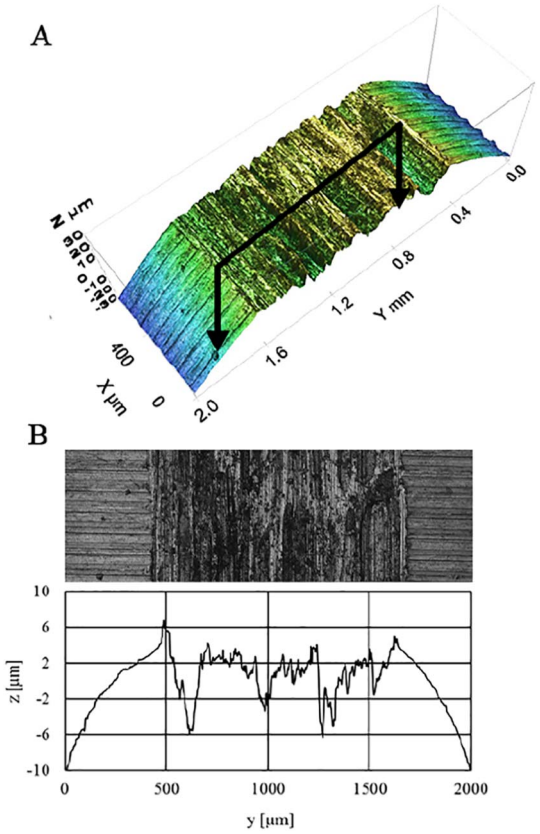

Fig. 6. A) Profiler image of the worn area of the wrought sample machined in dry conditions; B) Section profile in correspondence of the area highlighted in A).

Table 6
Average volume loss expressed in 10^{-3} mm^3 during the biotribological tests.

		OCP [V]	E = 0.2 [V]		
Ti6Al4V as-delivered state	Cutting condition	V_{tot}	V_{tot}	V_{wrac}	V_{mech}
Wrought	Dry	62 ± 6	86 ± 5	10.51 ± 1	75.5 ± 7
EBM	Dry	70 ± 3	88 ± 4	13.2 ± 1	74.8
Wrought	Wet	39 ± 8	42 ± 6	11.9 ± 1	30.1 ± 6
EBM	Wet	42 ± 7	45 ± 6	10.5 ± 1	34.5 ± 6
Wrought	Cryogenic	40 ± 10	43 ± 7	10.3 ± 1	32.7 ± 3
EBM	Cryogenic	37 ± 6	44 ± 7	7.37 ± 1	36.6 ± 6

accelerated corrosion was not taken into account being its contribution negligible. In general, as expected, the total wear volume from the tests carried out at an applied potential is higher than the one obtained during OCP tests, as a consequence of the enhancement of the corrosion induced by the sliding process. Another general consideration is that, since the Ti6Al4V alloy is a passive metal, mechanical wear mainly contributes to the tribocorrosion degradation whereas the wear accelerated corrosion is a small percentage of the total wear.

Both at OPC and at a passive potential, the total wear volume of the wrought and EBM samples are similar. Similar results were found by Licausi et al. [32], who studied the influence of the fabrication process as a function of the fluoride content in artificial saliva. They demonstrated that V_{mech} at an applied passive potential of 0.2 V in case of the sintered titanium was slightly higher than in case of casting attributing this evidence to the higher amount of asperities obtained during the powder metallurgy processing route.

A more significant effect can be found considering the cooling strategy: the sample machined in dry conditions presented nearly the double amount of wear volume compared to the wet and cryogenic machined samples. Both at OPC and at a passive potential, the dry machined EBM samples were characterized by the highest amount of wear while the cryogenic machined EBM samples by the lowest one. These outcomes are in accordance with the fact that the dry machined EBM sample presented the lowest potential value and the highest corrosion current value during sliding. This sample presented also the highest amount of wear accelerated by corrosion due to the fact that its corrosion potential was the lowest between the considered cases. On the contrary, the cryogenic machined samples had a sensible lower wear volume compared to the dry machined samples due to their improved surface properties. This is in accordance with the work by S. Bruschi et al. [17] who showed that cryogenic machining could be an efficient method to reduce friction and to assure the occurrence of a higher degree of adhesive wear rather than abrasive wear on the machined cylinders, therefore limiting the scratching of the underlying material and reducing the material loss. The wet machined samples are also characterized by a smaller volume of total wear compared to the dry machined ones. These is in accordance with the results of the characterization after machining that showed the improved surface integrity obtained by using a cutting fluid during machining compared to dry cutting.

The wear volume of the wet machined samples was found to be close to the one of the cryogenic machined ones, revealing a good wear behaviour. Anyway, the wet machined samples were characterized by a higher degree of wear accelerated corrosion that could increase in most aggressive environments, as in the presence of the toothpaste fluorides.

3.4. Wear characterization

The SEM images of the wear scars after the biotribological tests under OCP are shown in Fig. 7. The wear scars of the samples worn at E = 0.2 V are not included because they show similar characteristics to those collected at OCP.

Figures compare the Secondary Electron (SE) and Backscattered (BSED) detectors images recorded for each sample. The SE images are representative of the topography of the worn surfaces, while the BSED images add information about the surface chemical composition, namely chemical elements with different atomic number appear with different grey scale colours.

In general, different wear mechanisms can be detected, namely abrasive and adhesive wear, regardless of the processing route and cooling strategies. All of the images show uniform grooves aligned with the sliding direction and perpendicular to the machining feed marks that are representative of abrasive wear, but also some adhesive wear is present, revealed by the presence of patch of material of a different nature from the substrate.

By comparing the wear scars, it can be noticed that the amount of adhered material is higher for the wrought samples except in the case of the cryogenic machined one. These observations are in accordance with the amount of calculated wear volume: the EBM samples were in fact characterized by a higher amount of volume loss except in the cryogenic case. This can be ascribed to the fact that the presence of material from the counterpart can protect the underlying Ti6Al4V surface from further wear, reducing abrasion. Fig. 8A, in which a magnification of the wear scar of Fig. 7IIa is reported, confirms that: consistent adhered patches cover evenly the surface of the sample. It is worth to notice that these layers present micro-cracks perpendicular to the sliding direction as a consequence of the severe deformation they were subjected to.

Considering the influence of the cooling strategy, the dry machined samples presented wider and more fragmented wear scars, and were characterized by the presence of craters that developed as a consequence of the abrasion exerted by flakes of material removed from the surface. An example of these craters is shown in Fig. 8B, where a certain amount of wear debris can be also noticed, which could have enhanced the material wear [33].

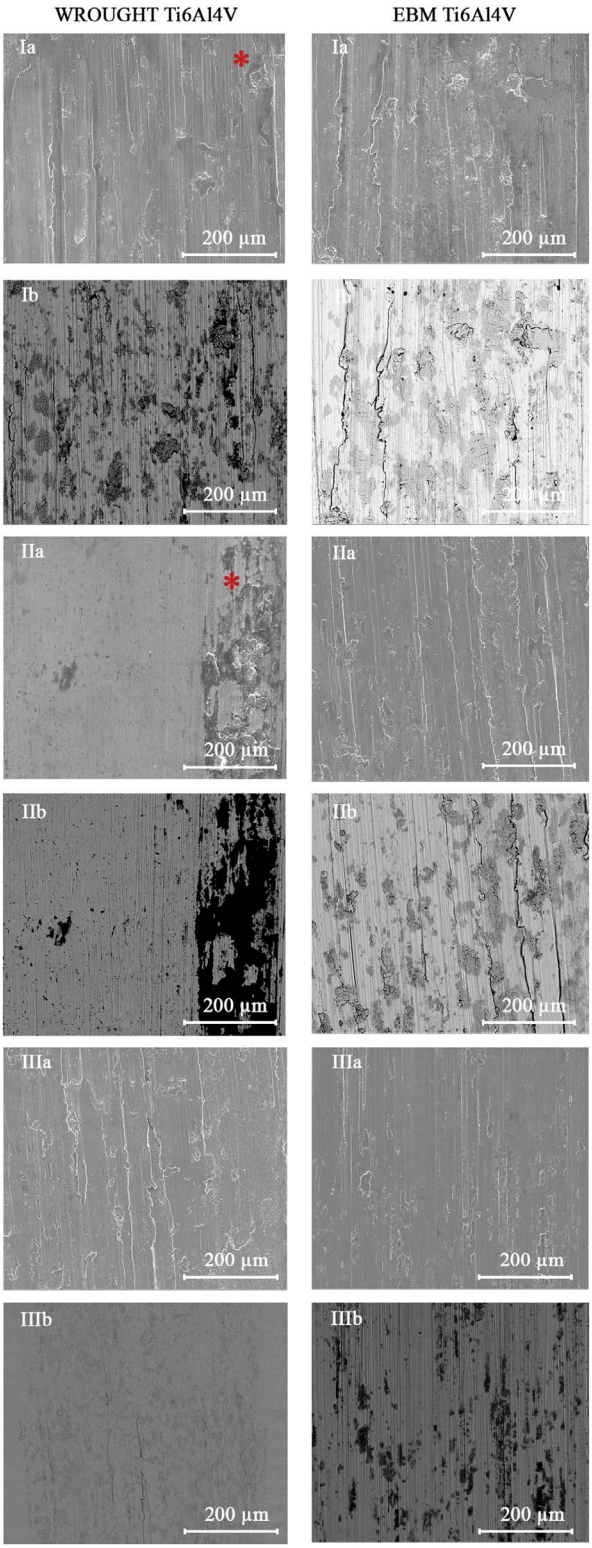

Fig. 7. SEM images of the wear scars at OCP. Key: a) SE images, b) BSED images, I) samples machined in dry conditions, II) samples machined in wet conditions, III) samples machined in cryogenic conditions.

The wear volume calculations showed that the dry machined samples were subjected to a double amount of volume loss compared to the cryogenic machined samples, which offered an improved wear behaviour thanks to their improved surface characteristics (see Table 3). This is in accordance with the Archard's wear rate law [34], which states that the volume of generated wear volume is inversely proportional to the hardness of the softest contacting surface.

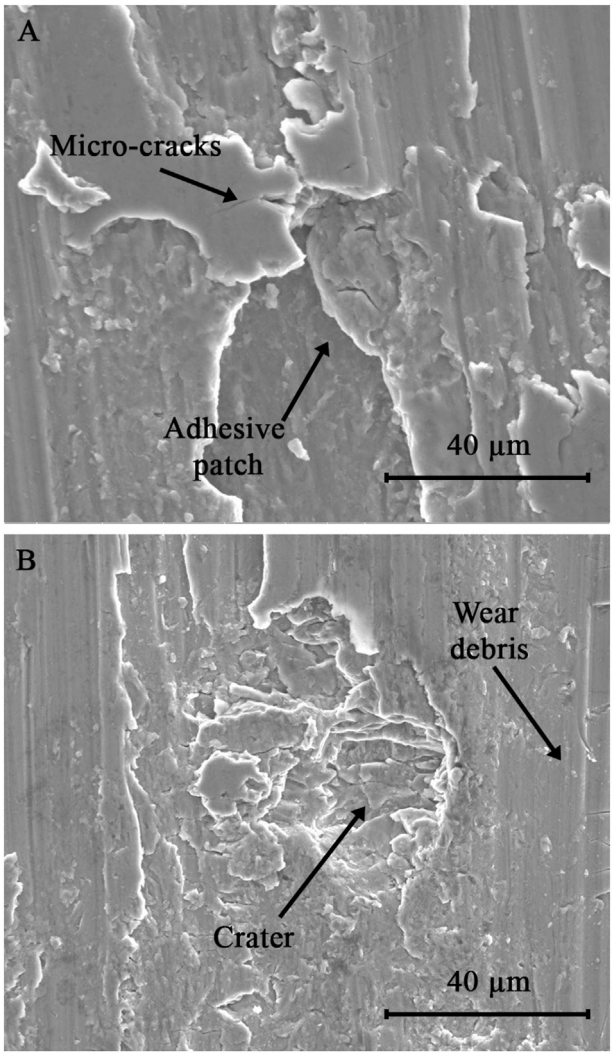

Fig. 8. Magnified images of the wear scars reported in Fig. 5: A) 2500 × image of the zone near the star in Fig. 5Ia; B) 2500 × image of the zone near the star in Fig. 5IIa.

4. Conclusions

In this work, the influence of the cooling conditions on the tribocorrosion behaviour of the Ti6Al4V titanium alloy obtained by two different fabrication process, namely wrought and Additive Manufactured through Electron Beam Melting, was investigated.

Tribocorrosion tests were carried in a wet and temperature-controlled experimental apparatus in which the Ti6Al4V samples were made to slid against zirconia plates in order to reproduce as much as possible the human mouth conditions.

The main results and conclusions obtained from this study can be summarized as follows:

- Cryogenic machining affected the surface properties of the EBM and wrought Ti_6Al_4V samples, inducing higher micro-hardness, higher compressive residual stresses and lower surface roughness than dry and wet cutting. The anodic polarization curves showed that the cryogenic machining also enhanced the corrosion behaviour properties, leading to the corrosion potential increase and corrosion current decrease. The increase in the corrosion performance was more evident for the EBM samples.
- The OCP values of the cryogenic machined samples recorded during the reciprocating sliding tests were arranged at a higher level

compared to the ones of the samples machined under wet and dry conditions, meaning they were less affected by the corrosive environment. This is a clear indication of enhanced tribocorrosion properties.

- The corrosion current values presented the same trend highlighted for the OCP values.
- The volume wear calculations confirmed the aforementioned results showing that the dry machined samples were characterized by a volume wear almost double compared to that of the cryogenic machined samples.
- The EBM samples presented an in-vitro behaviour similar to that of the wrought ones proving that this fabrication process can offer a suitable process route for manufacturing biomedical implants.

On the basis of these outcomes, it can be stated that cryogenic machining can represent a suitable method to produce wrought and EBM Ti6Al4V components for dental applications with enhanced tribocorrosion characteristics.

References

[1] I. Golvano, I. Garcia, A. Conde, W. Tato, A. Aginagalde, Influence of fluoride content and pH on corrosion and tribocorrosion behaviour of $Ti_{13}Nb_{13}Zr$ alloy in oral environment, J. Mech. Behav. Biomed. Mater. 49 (2015) 186–196, http://dx.doi.org/10.1016/j.jmbbm.2015.05.008.

[2] M. Long, H.J. Rack, Titanium alloys in total joint replacement-a materials science perspective, Biomaterials 19 (1998) 1621–1639, http://dx.doi.org/10.1016/S0142–9612(97)00146-4.

[3] A. Molinari, G. Straffelini, B. Tesi, T. Bacci, Dry sliding wear mechanisms of the $Ti_6A_{l4}V$ alloy, Wear 208 (1997) 105–112, http://dx.doi.org/10.1016/S0043–1648(96)07454-6.

[4] A.C. Vieira, A.R. Ribeiro, L.A. Rocha, J.P. Celis, Influence of pH and corrosion inhibitors on the tribocorrosion of titanium in artificial saliva, Wear 261 (2006) 994–1001, http://dx.doi.org/10.1016/j.wear.2006.03.031.

[5] M. Barry, D. Kennedy, K. Keating, Z. Schauperl, Design of dynamic test equipment for the testing of dental implants, Mater. Des. 26 (2005) 209–216, http://dx.doi.org/10.1016/j.matdes.2004.07.001.

[6] S. Mischler, A.I. Mun, Wear of CoCrMo alloys used in metal-on-metal hip joints: a tribocorrosion appraisal, Wear 297 (2013) 1081–1094, http://dx.doi.org/10.1016/j.wear.2012.11.061.

[7] I. Garcìa, D. Drees, J.P. Celis, Corrosion-wear of passivating materials in sliding contacts based on a concept of active wear track area, Wear 249 (2001) 452–460.

[8] S. Mischler, A. Spiegel, D. Landolt, The role of passive oxide films on the degradation of steel in tribocorrosion systems, Wear (1999) 1078–1087.

[9] M.T. Mathew, P.S. Pai, R. Pourzal, A. Fischer, M.A. Wimmer, Significance of tribocorrosion in biomedical applications: overview and current status, Adv. Tribol. 2009 (2009), http://dx.doi.org/10.1155/2009/250986.

[10] M.P. Licausi, Tribocorrosion mechanisms of Ti6Al4V biomedical alloys in artificial saliva with different pHs, J. Phys. 46 (2013) 404003–404,013, http://dx.doi.org/10.1088/0022–3727/46/40/404003.

[11] J.C.M. Souza, H.A. Tajiri, C.S. Morsch, M. Buciumeanu, M.T. Mathew, F.S. Silva, B. Henriques, Tribocorrosion behavior of $Ti_6A_{l4}V$ coated with a bio-absorbable polymer for biomedical applications, J. Bio- Tribo-Corrosion 1 (2015) 27, http://dx.doi.org/10.1007/s40735–015–0029-5.

[12] I. Hacisalihoglu, A. Samancioglu, F. Yildiz, G. Purcek, A. Alsaran, Tribocorrosion properties of different type titanium alloys in simulated body fluid, Wear 332–333 (2015) 1–8, http://dx.doi.org/10.1016/j.wear.2014.12.017.

[13] Z. Doni, A.C. Alves, F. Toptan, J.R. Gomes, A. Ramalho, M. Buciumeanu, L. Palaghian, F.S. Silva, Dry sliding and tribocorrosion behaviour of hot pressed CoCrMo biomedical alloy as compared with the cast CoCrMo and Ti6Al4V alloys, Mater. Des. 52 (2013) 47–57, http://dx.doi.org/10.1016/j.matdes.2013.05.032.

[14] A. Bordin, S. Bruschi, A. Ghiotti, P.F. Bariani, Analysis of tool wear in cryogenic machining of additive manufactured Ti6Al4V alloy, Wear 328–329 (2015) 89–99, http://dx.doi.org/10.1016/j.wear.2015.01.030.

[15] G. Rotella, O.W. D Jr., D. Umbrello, L. Settineri, The effects of cooling conditions on surface integrity in machining of $Ti_6A_{l4}V$ alloy, Int. J. Adv. Manuf. Technol. 71 (2014) 47–55, http://dx.doi.org/10.1007/s00170–013–5477-9.

[16] D. Umbrello, F. Micari, I.S. Jawahir, CIRP annals - manufacturing technology the effects of cryogenic cooling on surface integrity in hard machining: a comparison with dry machining, CIRP Ann. Manuf. Technol. 61 (2012) 103–106, http://dx.doi.org/10.1016/j.cirp.2012.03.052.

[17] S. Bruschi, R. Bertolini, A. Bordin, F. Medea, A. Ghiotti, Influence of the machining parameters and cooling strategies on the wear behavior of wrought and additive manufactured $Ti_6A_{l4}V$ for biomedical applications, Tribol. Int. 102 (2016) 133–142, http://dx.doi.org/10.1016/j.triboint.2016.05.036.

[18] R. Bertolini, S. Bruschi, A. Bordin, A. Ghiotti, L. Pezzato, M. Dabalà, Fretting corrosion behavior of additive manufactured and cryogenic-machined Ti6Al4V for biomedical applications, Adv. Eng. Mater. (2016) 1–9, http://dx.doi.org/10.1002/adem.201500629.

[19] N.F. von Maltzahn, J. Holstermann, P. Kohorst, Retention forces between titanium and zirconia components of two-part implant abutments with different techniques of surface modification, Clin. Implant. Dent. Relat. Res. (2015) 1–10, http://dx.doi.org/10.1111/cid.12352.

[20] M.J. Bermingham, S. Palanisamy, D. Kent, M.S. Dargusch, A comparison of cryogenic and high pressure emulsion cooling technologies on tool life and chip morphology in Ti–6Al–4V cutting, J. Mater. Process. Technol. 212 (2012) 752–765, http://dx.doi.org/10.1016/j.jmatprotec.2011.10.027.

[21] X.C. Zhanga, Y.K. Zhang, J.Z. Lu, F.Z. Xuan, Z.D. Wang, S.T. Tu, Improvement of fatigue life of Ti–6Al–4V alloy by laser shock peening, Mater. Sci. Eng. A 527 (2010) 3411–3415.

[22] E. Bressan, D. Lops, C. Tomasi, S. Ricci, M. Stocchero, E.L. Carniel, Experimental and computational investigation of Morse taper conometric system reliability for the definition of fixed connections between dental impants and prostheses, J. Eng. Med. 228 (2014) 674–681, http://dx.doi.org/10.1177/0954411914545556.

[23] M. Dhananchezian, M. Pradeep Kumar, Cryogenic turning of the Ti-6Al-4V alloy with modified cutting tool inserts, Cryogenics 51 (2011) 34–40, http://dx.doi.org/10.1016/j.cryogenics.2010.10.011.

[24] I. Wstawska, K. Ślimak, The influence of cooling techniques on cutting forces and surface roughness during cryogenic machining of titanium alloys, Arch. Mech. Technol. Mater. (2016) 12–17, http://dx.doi.org/10.1515/amtm-2016-0003 (0).

[25] J.C. Outeiro, A.C. Batista, M.J. Marques, Residual stresses induced by dry and cryogenic cooling during machining of AZ31B magnesium alloy, Adv. Mater. Res. 996 (2014) 658–663, http://dx.doi.org/10.4028/www.scientific.net/AMR.996.658.

[26] F. Pusavec, H. Hamdi, J. Kopac, I.S. Jawahir, Surface integrity in cryogenic machining of nickel based alloy-Inconel 718, J. Mater. Process. Technol. 211 (2011) 773–783, http://dx.doi.org/10.1016/j.jmatprotec.2010.12.013.

[27] P.R. Roberge, Handbook of Corrosion Engineering, Mc-Graw-Hill, New York, 2000.

[28] G 102-89 Standard: Standard Practice for Calculation of Corrosion Rates and Related Information from Electrochemical Measurements, United States, (1999).

[29] O. Takakuwa, H. Soyama, Effect of residual stress on the corrosion behavior of austenitic stainless steel, Adv. Chem. Eng. Sci. 5 (2015) 62–71.

[30] Y.Y. Wan, Stress influence on corrosion resistance of aluminium alloy surface, Adv. Mater. Res. 1017 (2014) 287–291, http://dx.doi.org/10.4028/www.scientific.net/AMR.1017.287.

[31] A. Bazzoni, S. Mischler, N. Espallargas, Tribocorrosion of pulsed plasma-nitrided cocrmo implant alloy, Tribol. Lett. 49 (2013) 157–167, http://dx.doi.org/10.1007/s11249–012–0047-0.

[32] M.P. Licausi, A. Igual Muñoz, V. Amigó Borrás, Influence of the fabrication process and fluoride content on the tribocorrosion behaviour of Ti6Al4V biomedical alloy in artificial saliva, J. Mech. Behav. Biomed. Mater. 20 (2013) 137–148, http://dx.doi.org/10.1016/j.jmbbm.2013.01.019.

[33] R.A. Buchanan, E.D. Rigney, J.M. Williams, Wear-accelerated corrosion of Ti-6Al-4V and nitrogen-ion-implanted Ti-6Al-4V: mechanisms and influence of fixed-stress magnitude, J. Biomed. Mater. Res. 21 (1987), http://dx.doi.org/10.1002/jbm.820210309.

[34] J.F. Archard, Contact and rubbing of flat surfaces, J. Appl. Phys. 24 (1953) 981, http://dx.doi.org/10.1063/1.1721448.